Ab initio melting curve of molybdenum by the phase coexistence method

C. Cazorla and M. J. Gillan
London Centre for Nanotechnology, UCL, London WC1H OAH, United Kingdom
and Department of Physics and Astronomy, UCL, London WC1E 6BT, United Kingdom

S. Taioli
Department of Earth Sciences, UCL, London WC1E 6BT, United Kingdom

D. Alfè
London Centre for Nanotechnology, UCL, London WC1H OAH, United Kingdom
and Department of Physics and Astronomy and Department of Earth Sciences, UCL,
London WC1E 6BT, United Kingdom

Ab initio calculations of the melting curve of molybdenum for the pressure range 0–400 GPa are reported. The calculations employ density functional theory (DFT) with the Perdew-Burke-Ernzerhof exchange-correlation functional in the projector augmented wave (PAW) implementation. Tests are presented showing that these techniques accurately reproduce experimental data on low-temperature body-centered cubic (bcc) Mo, and that PAW agrees closely with results from the full-potential linearized augmented plane-wave implementation. The work attempts to overcome the uncertainties inherent in earlier DFT calculations of the melting curve of Mo, by using the "reference coexistence" technique to determine the melting curve. In this technique, an empirical reference model (here, the embedded-atom model) is accurately fitted to DFT molecular dynamics data on the liquid and the high-temperature solid, the melting curve of the reference model is determined by simulations of coexisting solid and liquid, and the *ab initio* melting curve is obtained by applying free-energy corrections. The calculated melting curve agrees well with experiment at ambient pressure and is consistent with shock data at high pressure, but does not agree with the high-pressure melting curve deduced from static compression experiments. Calculated results for the radial distribution function show that the short-range atomic order of the liquid is very similar to that of the high-*T* solid, with a slight *decrease* of coordination number on passing from solid to liquid. The electronic densities of states in the two phases show only small differences. The results do not support a recent theory according to which very low dT_m/dP values are expected for bcc transition metals because of electron redistribution between *s-p* and *d* states. © *2007 American Institute of Physics*. [DOI: 10.1063/1.2735324]

I. INTRODUCTION

Over the past five years, a major controversy has developed about the high-pressure melting curves of transition metals. According to static compression experiments, performed using diamond anvil cells (DAC) at pressures from ambient up to ~100 GPa (1 Mbar), the melting temperatures T_m of many transition metals, particularly those having the body-centered cubic (bcc) crystal structure, changes by no more than a few hundred Kelvin over this pressure range.[1,2] In some cases, this finding seems to be in gross conflict with shock experiments, which indicate an increase of T_m of several thousand Kelvin over the same pressure range.[3–5] Theoretical work[6–9] based directly or indirectly on density functional theory (DFT) generally supports the shock data. We report here a detailed DFT study of the high-pressure melting curve of Mo, a metal for which there are some of the largest differences between DAC measurements and other data (see, e.g., Fig. 2 in Ref. 10).

There has already been quite extensive theoretical work on the high-*P* melting of metals. Some of this has been motivated by the desire to understand the properties of solid and liquid Fe in the Earth's core.[11] DFT-based calculations of the Fe melting curve[12–15] up to the pressure at the boundary between the solid inner core and the liquid outer core provide one of the important ways of constraining the temperature distribution in the core. Disagreements with DAC measurements on Fe and other transition metals are cause for concern, because if DFT were shown to be seriously in error, the reliability of DFT for the study of planetary interiors would be called into question. But, even without this practical motivation, a major disagreement between DFT predictions and experimental data must be taken seriously, because it suggests an unexpected failure either of commonly used DFT approximations, or of apparently well-established experimental techniques. Reassuringly, DFT melting curves agree very closely with experiment for some metals, including Al (Refs. 16 and 17) and Cu.[18] The large disagreements arise mainly for transition metals, and the suggestion is that they are linked to *d*-band bonding.

Since the melting slope dT_m/dP is equal by the Clausius-Clapeyron relation to V^{ls}/S^{ls}, where V^{ls} and S^{ls} are the volume and entropy of fusion, respectively, and since S^{ls}

is unlikely to have exceptionally large values, a very low dT_m/dP is likely to be due to a low volume of fusion. It has been argued[1,19] that a low V^{ls} might be expected for bcc transition metals, because the liquid may be more close packed than the solid. But, recently, an additional argument has been advanced for low dT_m/dP values.[20] This argument depends on the fact that the distribution of conduction electrons between *s-p* states and *d* states is known to depend on the degree of compression and on the crystal stucture.[21,22] The suggestion is that the (assumed) change of coordination on going from bcc solid to liquid leads to a change of electronic structure, and hence a change in the electron distribution between *s-p* and *d* states, and that this redistribution stabilizes the liquid and lowers T_m. One of the important purposes of the present work is to use DFT molecular dynamics (MD) simulations to test these suggestions for the case of Mo.

There has been previous DFT work[6,9] on the high-pressure melting of Mo. The early work of Moriarty[6] employed a many-body total energy function derived from first-principles "generalized pseudopotential theory."[23] This approximates the total energy of the system in terms of volume-dependent 1-, 2-, 3-, and 4-body interatomic potentials, and accounts for the angular forces that are known to be important in transition metals. This form of total-energy function is designed to be fully transferable between different structures, and should be valid for both the solid and the liquid state. The model total-energy function was used in MD simulations to determine the melting curve by two methods. The first method consisted of cycling the simulated system up and down through the melting point at fixed volume. The results were cross checked against a second method based on the calculation of the free energies of the solid and the liquid. This was pioneering work, but its quantitative accuracy can be questioned, because some of the phonon frequencies predicted by the total energy function agreed rather poorly with experiment. In addition, the surprising claim was made that T_m could be changed by up to a factor of 2 by the inclusion of thermal electronic excitations, which were treated only crudely. The predicted melting curve was consistent with shock data, but was far above the curve given by recent DAC measurements: the difference of T_m values amounts to $\sim$3000 K at $P=100$ GPa. Much more recently, direct DFT MD simulation has been used by Belonoshko *et al.*[9] to map out the Mo melting curve up to $P \simeq 330$ GPa. Their melting curve, like that of Moriarty,[6] is consistent with shock data, but disagrees strongly with DAC data. However, even though the simulations employed an implementation of DFT that is expected to be accurate, the method used to map the melting curve may still give inaccurate results, as noted by the authors. Their method was to heat the simulated solid at constant volume until the internal energy, pressure, radial distribution function, and self-diffusion coefficient showed discontinuities attributable to melting. This approach gives an upper bound to T_m, but may overestimate it significantly, because of superheating. The authors estimated that the error in T_m due to superheating should be $\sim$20%, but the arguments for this estimate are indirect.

The present new work on Mo melting has several aims.

The first aim is to calculate more accurately the melting curve that follows from the adopted DFT exchange-correlation functional E_{xc}. (We present tests showing that the GGA-PBE functional is a good choice.) It is only by doing this that the possible reasons for the disagreement between theory and experiment can be narrowed down. We have shown in our recent work on other materials that the errors in computed DFT T_m values can be reduced to a few percent, and we have described several techniques for doing this.[11] The technique used here is the "reference coexistence method."[24] This requires the accurate fitting of an empirical "reference" total energy function to DFT MD simulations on the solid and the liquid; the melting curve of the reference model is then calculated from simulations on large systems consisting of coexisting solid and liquid; as an essential last step, free-energy corrections for the difference between the reference and DFT total-energy functions are used to correct the melting curve. This technique was successfully used in our work on the melting of Cu,[18] and it has been shown to give results in excellent agreement with an alternative technique, in which DFT free energies of the solid and liquid are calculated.[12,24] Since it is a "thermodynamic" technique relying on equality of Gibbs free energies of the two phases, it cannot suffer from superheating problems. A second important aim is to study the differences of atomic and electronic structure of the coexisting solid and liquid, to provide an improved understanding of the factors that determine the melting curve of Mo. The empirical reference model used to determine the DFT melting curve has the form of the embedded atom model (EAM).[25,26] A useful side benefit of the work is that we obtained a parametrized EAM that mimics quite well the DFT total-energy function of high-T solid and liquid Mo. This model reveals important features of the energetics of Mo at high P and high T, and we expect it to be useful in future modeling work on this metal.

The remainder of the paper is organized as follows. A brief summary of the DFT modeling techniques is given in Sec. II, followed by an outline of the reference coexistence technique. Then, Sec. III details the rather extensive tests we have performed to ensure that the techniques deliver an accurate description of the energetics and the vibrational and electronic properties of Mo. Section IV presents our results for the DFT melting curve of Mo up to 400 GPa, together with the entropy and volume of fusion as a function of pressure; our comparison of the atomic and electronic structures of the high-T bcc solid and the liquid is reported at the end of the section. A discussion of all the results and their relation with previous work is given in Sec. V, followed by our conclusions.

II. TECHNIQUES

A. DFT methods

A comprehensive description of DFT methods as applied to the modeling of condensed matter is given in recent books.[27,28] As is well known, there is one and only one uncontrollable approximation in DFT, namely the approximation used for the exchange-correlation functional E_{xc}. There is abundant evidence that commonly used E_{xc} functionals

yield accurate results for a range of properties of transition-metal crystals, including equilibrium lattice parameter, elastic constants, phonon frequencies, $T=0$ equation of state, solid-state phase boundaries, etc.[11] DFT provides the basis for our present understanding of the electronic structure of transition-metal crystals as a function of pressure. There is also some evidence that it accurately reproduces the structure of liquid transition metals.[29] Nevertheless, we considered it necessary to test the accuracy of different E_{xc} in the case of Mo, as we report in Sec. III.

A completely separate issue from the choice of E_{xc} is the *implementation* of DFT that is used. This concerns mainly the way that the electron orbitals are represented. For simulations of the high-T solid and the liquid, DFT molecular dynamics (MD) must be used, and for this we use the PAW (projector augmented wave) technique,[30,31] which is generally regarded as the most accurate for MD purposes. The PAW method developed by Blöchl[30] efficiently combines some of the features originally devised within both linear augmented-plane-wave (LAPW, briefly described below) and pseudopotential approaches. In PAW, a linear transformation between the all-electron and "pseudized" wave functions is defined in terms of all-electron and pseudized partial waves and a set of projector functions localized on the atoms. There is a simple formal relationship between PAW and the ultrasoft pseudopotential method of Vanderbilt,[32] and computationally the two approaches are almost equivalent.[31]

For MD, we use the method known as Born-Oppenheimer dynamics, in which the self-consistent ground state is recalculated at each new MD time-step. Given the criticisms that are sometimes made of DFT work on melting properties,[10] it is important to be clear that this means the recalculation of the electronic structure of the entire simulated system, so that changes of electronic structure on going from solid to liquid at any degree of compression are fully included. Although PAW is well suited to MD simulation, we regard it as essential to check its accuracy against still more accurate implementations of DFT, and to do this we have compared with the predictions of the FP-LAPW (full-potential linearized augmented plane-wave) technique, which was developed for high-precision calculations on crystals.[33–35] In this approach, space is divided into spherical regions centered on the ions, and the interstitial space between the spheres. Accurate solution of Schrödinger's equation on a radial grid for each angular momentum within each sphere allows both valence and core states to be treated to arbitrarily high precision. The FP-LAPW results to be presented include fully relativistic treatment of the core states and scalar relativistic treatment of the states in valence.[36] In FP-LAPW calculations on crystalline Mo, we can ensure that they are fully converged with respect to all technical parameters, so that all errors of implementation are negligible, and the only approximation is that due to E_{xc} itself. All our PAW and FP-LAPW calculations were performed using the VASP code[37] and the WIEN2K code,[38] respectively.

Normally, the aim of DFT calculations is to obtain the electronic ground state for given ionic positions. However, because of the high T involved, it is essential in the present work to include thermal electronic excitations, so that for any given ionic positions we must determine the orbitals and occupation numbers that self-consistently minimize the electronic *free* energy, using the $T>0$ version of DFT originally developed by Mermin.[39] We know this is essential, because work on other transition metals[40] shows that the electronic specific heat becomes comparable with the vibrational contribution for $T \sim 5000$ K. Without this, the free-energy difference between solid and liquid might be seriously in error. All our MD simulations are done in the canonical (N,V,T) ensemble,[42] with the electronic T set equal to the T of the ensemble.

Values of technical parameters (k-point sampling, plane-wave cutoff, etc.) will be given when we present the calculations.

B. Reference coexistence methods

There are three steps in the reference coexistence technique.[24] First, an empirical reference model is fitted to *ab initio* simulations of the solid and the liquid at thermodynamic states close to the expected melting curve. Then, the reference model is used to perform simulations on large systems in which solid and liquid coexist, so as to obtain points on the melting curve of the model. Finally, the differences between the reference and *ab initio* total energy functions are used to correct the melting properties of the fitted model so as to obtain the *ab initio* melting properties.

In this work, we have used the embedded-atom model (EAM) (Refs. 25 and 26) as the reference model. The total energy function U_{ref} of this model for a system of N atoms has the form

$$U_{ref}(\mathbf{r}_1, \mathbf{r}_2, \dots \mathbf{r}_N)$$
$$= \frac{1}{2}\varepsilon \sum_{i \neq j} \left(\frac{a}{r_{ij}}\right)^n - C\varepsilon \sum_i \left[\sum_{j(\neq i)} \left(\frac{a}{r_{ij}}\right)^m \right]^{1/2}, \quad (1)$$

where $r_{ij} = |\mathbf{r}_i - \mathbf{r}_j|$ is the separation of atoms i and j. The first term on the right represents an inverse-power repulsive pair potential, while the second (embedding) term describes the d-band bonding. The model is specified by the characteristic length a, the energy scale ε, the dimensionless coefficient C characterizing the strength of the embedding energy, and the embedding and repulsive exponents m and n. We wish $U_{ref}(\mathbf{r}_1, \dots \mathbf{r}_N)$ to mimic as closely as possible the *ab initio* total energy function $U_{AI}(\mathbf{r}_1, \dots \mathbf{r}_N)$, and we achieve this by adjusting the EAM parameters.

The method for fitting U_{ref} to U_{AI} is designed so as to minimize the corrections to the melting curve caused by the difference $\Delta U \equiv U_{AI} - U_{ref}$. We therefore recall the correction scheme before describing the fitting itself. For given P and T, the difference $G_{AI}^{ls} \equiv G_{AI}^l - G_{AI}^s$ between the Gibbs free energies of the *ab initio* liquid and solid deviates from the corresponding difference $G_{ref}^{ls} \equiv G_{ref}^l - G_{ref}^s$ of the reference liquid and solid, and we write

$$G_{AI}^{ls}(P,T) = G_{ref}^{ls}(P,T) + \Delta G^{ls}(P,T). \quad (2)$$

It is the shift $\Delta G^{ls}(P,T)$ caused by changing the total-energy function from U_{ref} to U_{AI} that causes the shift of melting temperature at given pressure. To first order, the latter shift is[24]

$$T'_m = \frac{\Delta G^{ls}(T_m^{\text{ref}})}{S_{\text{ref}}^{ls}}, \tag{3}$$

where S_{ref}^{ls} is the difference between the entropies of liquid and solid (i.e., the entropy of fusion) of the reference system, and $\Delta G^{ls}(T_m^{\text{ref}})$ is ΔG^{ls} evaluated at the melting temperature of the reference system.

The shift ΔG^{ls} is the difference of shifts of Gibbs free energies of liquid and solid caused by the shift $\Delta U \equiv U_{\text{AI}} - U_{\text{ref}}$ of total energy function. We find it convenient to perform our simulations at constant volume and temperature. Under these conditions, the shift of Helmholtz free energy ΔF arising from ΔU is given by the well-known expansion

$$\Delta F = \langle \Delta U \rangle_{\text{ref}} - \tfrac{1}{2}\beta \langle \delta\Delta U^2 \rangle_{\text{ref}} + \cdots, \tag{4}$$

where $\beta \equiv 1/k_{\text{B}}T$, $\delta\Delta U \equiv \Delta U - \langle \Delta U \rangle_{\text{ref}}$, and the averages are taken in the reference ensemble. From ΔF, we obtain the shift of Gibbs free energy at constant pressure as

$$\Delta G = \Delta F - \tfrac{1}{2}V\kappa_T(\Delta P)^2, \tag{5}$$

where κ_T is the isothermal compressibility and ΔP is the change of pressure when U_{ref} is replaced by U_{AI} at constant V and T.

In fitting the EAM U_{ref} to the *ab initio* U_{AI} so as to minimize the corrections we have just described, we see from Eqs. (4) and (5) that the effects of $\langle \Delta U \rangle_{\text{ref}}$, $\langle \delta\Delta U^2 \rangle_{\text{ref}}$, and ΔP all need to be made small. Concerning $\langle \Delta U \rangle_{\text{ref}}$, we note that addition of a position-independent constant to either U_{AI} or U_{ref} has no effect on the properties of the solid or the liquid, since it simply redefines the energy zero, so that a large value of $\langle \Delta U \rangle_{\text{ref}}$ is not in itself significant. However, it is crucially important that $\langle \Delta U \rangle_{\text{ref}}$ should have almost the same value in the solid and the liquid, because otherwise there would be a large shift of ΔG^{ls}. We also seek to make $\langle \delta\Delta U^2 \rangle_{\text{ref}}$ and ΔP small in both phases. To satisfy all these requirements, we perform long *ab initio* MD simulations of the solid and the liquid at thermodynamic states near the expected melting curve. A large number of statistically independent configurations are then drawn from both these runs, so that we get a large set of U_{AI} values for a collection of configurations representative of the solid and the liquid. Our procedure is then to minimize the mean square fluctuations of ΔU over this whole set: with $\overline{\Delta U}$ the mean value of ΔU over the whole set, we minimize $\overline{\delta\Delta U^2}$, where $\delta\Delta U \equiv \Delta U - \overline{\Delta U}$. Note that this $\overline{\delta\Delta U^2}$ is not the same quantity as the $\langle \delta\Delta U^2 \rangle_{\text{ref}}$ appearing in Eq. (4), because $\overline{\delta\Delta U^2}$ characterizes the fluctuations of ΔU over a set of configurations drawn from both liquid and solid. Minimization of $\overline{\delta\Delta U^2}$ has the effect of reducing simultaneously the difference of $\langle \Delta U \rangle_{\text{ref}}$ between solid and liquid, and of reducing $\langle \delta\Delta U^2 \rangle_{\text{ref}}$ in the two phases. In order to reduce also ΔP^2 in the two phases, we add ΔP^2 into the quantity to be minimized, with a suitable weight. As will be described in Sec. IV A, we find it necessary to refit the EAM in this way for different ranges of pressure along the melting curve. A convenient way of characterizing the quality of fit of U_{ref} to U_{AI} is obtained by dividing $\overline{\delta\Delta U^2}$ by the mean square value of the fluctuation of *ab initio* energy $\delta U_{\text{AI}} \equiv U_{\text{AI}} - \overline{U_{\text{AI}}}$, where $\overline{U_{\text{AI}}}$ is the *ab initio*

energy averaged over the collection of solid and liquid configurations. The dimensionless quantity characterizing the fit is then $\psi \equiv [\overline{\delta\Delta U^2}/\overline{\delta U_{\text{AI}}^2}]^{1/2}$; the smaller the value of ψ, the better is the fit.

Following our previous work,[16,18,24] our simulations of coexisting solid and liquid with the reference model are performed in the (N, V, E) ensemble. Starting with a supercell containing the perfect bcc crystal, we thermalize it at a temperature slightly below the expected melting temperature. The system remains in the solid state. The simulation is then halted, and the positions of the atoms in one half of the supercell are held fixed, while the other half is heated to a very high temperature (typically eight times the expected melting temperature), so that it melts completely. With the fixed atoms still fixed, the molten part is then rethermalized to the expected melting temperature. Finally, the fixed atoms are released, thermal velocities are assigned, and the whole system is allowed to evolve freely at constant (N, V, E) for a long time (normally more than 60 ps), so that the solid and liquid come into equilibrium. The system is monitored by calculating the average number of particles in slices of the cell taken parallel to the boundary between the solid and liquid. With this protocol, there is a certain amount of trial and error to find the overall volume that yields the coexisting solid and liquid system. (An example of the density profile obtained when the two phases are in stable coexistence will be given in Sec. IV.) Our main simulations were done on cells containing 6750 atoms, constructed as a $15 \times 15 \times 30$ bcc supercell, the long axis being perpendicular to the initial liquid-solid boundary. We tested the adequacy of this system size by repeating the simulations with larger systems (around 10 000 atoms), and found no change in the results.

Finally, our best value of the *ab initio* melting temperature is obtained by adding to the reference melting temperature the correction T'_m given by Eq. (3). The reference entropy of fusion S_{ref}^{ls} needed in this equation is obtained by performing independent reference MD simulations of the solid and the liquid in the (N, V, T) ensemble at the temperatures at which we made the coexistence simulations, using at each of these temperatures the solid and liquid volumes that yield the coexistence pressure. These simulations give the enthalpy of fusion H_{ref}^{ls}, from which we obtain S_{ref}^{ls} from the relation $H_{\text{ref}}^{ls} = T_m^{\text{ref}} S_{\text{ref}}^{ls}$. To obtain the values of $\Delta G^{ls}(T_m^{\text{ref}})$ needed in Eq. (3), we again perform reference MD simulations of solid and liquid at the coexistence temperatures and volumes, and calculate U_{AI} for a statistically independent set of configurations drawn from these simulations. These U_{AI} values must, of course, be fully converged with respect to system size and **k**-point sampling. We find that for a system of 125 atoms and with U_{AI} calculated with a $2 \times 2 \times 2$ **k**-point grid for both solid and liquid, U_{AI} is converged within 5 meV/atom. These U_{AI} values are then used to compute $\langle \Delta U \rangle_{\text{ref}}$ and $\langle \delta\Delta U^2 \rangle_{\text{ref}}$. The same calculations yield ΔP for solid and liquid, which we use in Eq. (5).

III. TESTS OF METHODS: ZERO TEMPERATURE

To assess the accuracy of the techniques, we have carried out a number of tests on the zero-temperature crystal in
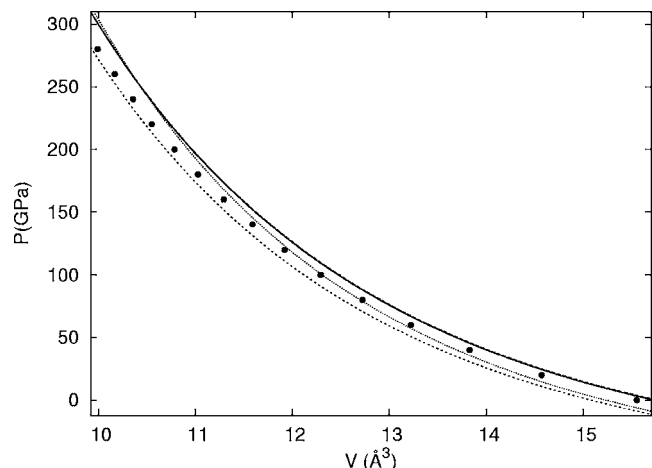
FIG. 1. Comparison of LDA and GGA pressure P as function of volume V for bcc Mo from the PAW method with different exchange-correlation functionals and valence sets. Long-dashed and solid lines (practically coincident) show GGA results with and without $4s$ states in the valence set. Short-dashed and dotted lines show LDA results with and without $4s$ states in the valence set. Dots show experimental results (Ref. 5).

FIG. 2. Comparison between PAW and FP-LAPW results for the GGA(PBE) and LDA(CA) approximations for E_{xc}. Solid and dashed curves show GGA(PBE) and LDA(CA) FP-LAPW results, respectively; short-dashed and dotted curves show GGA(PBE) and LDA(CA) PAW calculations, respectively. Solid dots show experimental data (Ref. 5).

the pressure range 0–300 GPa. There are three important questions to analyze. First, we want to test the accuracy of different exchange-correlation functionals compared with experimental data. Second, we aim to study the effect on PAW results of including different electronic states in the valence set. Third, FP-LAPW calculations are performed to assess errors incurred by the PAW approximation. In addition, we have done tests to demonstrate that PAW correctly reproduces the changes of electronic structure with pressure given by the FP-LAPW method. Tests of phonon frequencies are also carried out, because of their relevance to the vibrational free energy of the system.

A. PAW and FP-LAPW calculations

At very high pressures, states that would normally be treated as core states may respond significantly to compression. In the case of Mo, the $4p$ states lie only ~35 eV below the Fermi energy E_F and we always include them in the valence set. The $4s$ states lie considerably deeper at ~61 eV below E_F, and we have examined the effect of including them. We show in Fig. 1 PAW results for the pressure as a function of volume at $T=0$ K, with and without the $4s$ states included in the valence set, compared with experimental data.[5] Results are shown with both LDA (Ceperley-Alder parametrization[43]) and GGA (Perdew-Burke-Ernzerhof form[44]) exchange-correlation functionals. All calculations were performed on a primitive bcc cell, with a $32 \times 32 \times 32$ **k**-point grid and with energy cutoffs of 224.5 eV (without $4s$ states) and 287.6 eV (with $4s$ states); these settings ensure energy convergence to better than 1 meV/atom. With LDA, inclusion of $4s$ states makes a significant difference, and improves the agreement with experiment at high pressure, but with GGA the effect of including $4s$ states is very small. All the approximations deviate noticeably from experiment. At low pressures, LDA underestimates the volume by 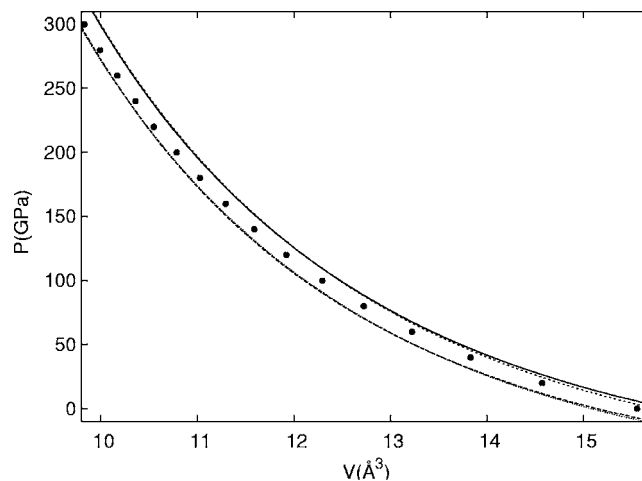about 3.1%, while GGA overestimates it by 1.2%. At high pressures, $P \sim 300$ GPa, LDA volumes are only 0.6% below measured values, while GGA continues to overestimate them by about 1.7%.

To check the accuracy of PAW itself, we have compared with FP-LAPW calculations of the $T=0$ K $P(V)$ relation, performed with the WIEN2K code.[38] Our FP-LAPW calculations include fully relativistic effects of the core states and scalar relativistic treatment of the states in valence,[36] and the tolerances are chosen so as to ensure energy convergence to better than 1 meV/atom.[45] As shown in Fig. 2, the FP-LAPW $P(V)$ results are almost indistinguishable from the PAW results over the entire pressure range of interest, with both LDA and GGA functionals. This provides valuable confirmation of the accuracy of the PAW technique, on which all our present calculations of melting properties are based. Out of interest, we also performed FP-LAPW calculations using the recently developed Wu-Cohen form of GGA,[46] which has been reported to give improved predictions of condensed-matter properties. This functional satisfies the same constraints used to construct the PBE functional, but the enhancement factor entering the exchange energy density is chosen to match closely the gradient expansion of Svendsen and von Barth[47] for systems having a slowly varying density. For this reason, this functional is expected to perform well for solids but not so well for atoms or molecules, where the variation of the valence electron density is generally larger. We find that this functional is in much better agreement with the experimental $P(V)$ data than either LDA or GGA(PBE). Unfortunately, at the time most of the present work was done, we had no way of performing Wu-Cohen calculations within PAW, so we were unable to do melting calculations with this new functional.

B. Electronic density of states

The electronic structure of transition metals has been intensively studied, and changes of electronic structure with increasing pressure have been thoroughly investigated both experimentally and theoretically.[21,22,48,49] The energetics of
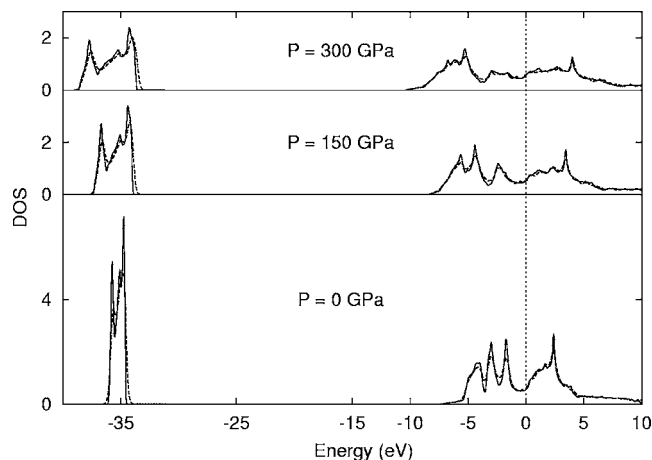
FIG. 3. Density of electronic states obtained with the PAW (dashed line) and FP-LAPW (solid line) at zero temperature and 0, 150, and 300 GPa. Fermi energies are shifted to zero (dotted line).

these metals is, of course, strongly dominated by the *d* bands, but the *s-p* bands also play an important role. An effect that has been well recognized for many years is the pressure-induced upward shift of the *s-p* band relative to the *d* band, caused by the greater spatial extent of the *s-p* orbitals.[21] This relative shift means that increasing pressure causes a transfer of electrons from *s-p* to *d* bands, resulting in an increase of occupancy of the latter. It has been proposed recently[10,20] that the large differences between theoretical predictions of melting curves and the results of static compression experiments for some transition metals may be due to an incorrect treatment of *s-p*→*d* transfer in the DFT-based simulations. In order to demonstrate that our PAW calculations reproduce the electronic structure as given by the most accurate DFT

methods, we have made detailed comparisons of the electronic density of states (DOS) calculated with PAW and FP-LAPW over the pressure range 0–300 GPa.

We show in Fig. 3 the electronic DOS from FP-LAPW and PAW calculated at 0, 150, and 300 GPa, using the GGA(PBE) functional. We note the essentially perfect agreement between the two methods. At all pressures, the DOS consists of two separate parts: a narrow peak at about 35 eV below the Fermi energy, corresponding to 4*p* states, and a much broader distribution consisting of the multiple peaks due to the 4*d* bands superimposed on the slowly varying DOS of the *s-p* bands. We note the characteristic feature of bcc transition metals that the Fermi energy falls in a deep minimum in the *d*-band DOS. As expected, the widths of the 4*p* and 4*d* parts of the DOS broaden markedly with increasing pressure. The pressure-induced relative shift of *s-p* and *d* bands cannot be clearly seen from the DOS itself. However, it is very clear from the band structure, shown at pressures of 0 and 300 GPa in Fig. 4. The state lying ~7 eV below the Fermi energy is the bottom of the *s-p* band, which lies well below the *d* states at zero pressure, but well above the lowest *d* states at $P=300$ GPa. We have checked that this relative shift is precisely reproduced by the PAW calculations. This leaves little doubt that the PAW techniques, on which all our melting calculations are based, correctly reproduce this important feature of the pressure dependent electronic structure. In Sec. IV, we will present results on the temperature dependence of the electronic DOS in the solid and the liquid.

C. Phonon frequencies

The calculation of phonon frequencies is an important test of DFT approximations, because of the detailed compari-
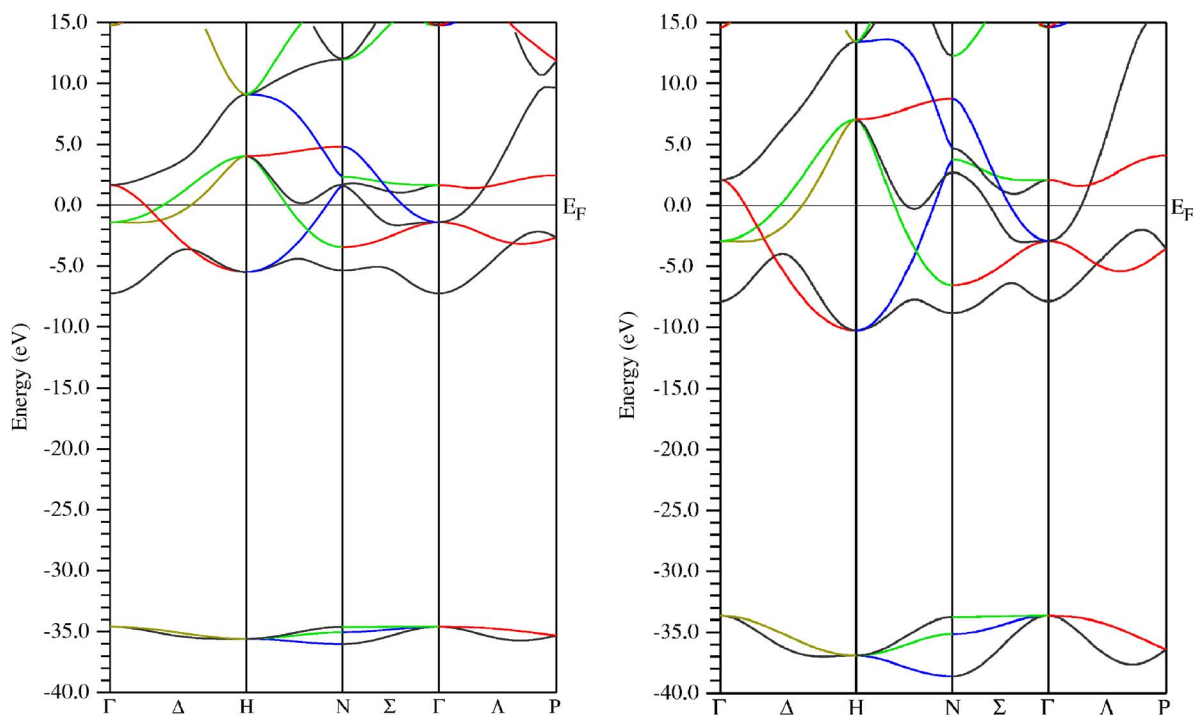

FIG. 4. FP-LAPW calculation of the energy bands of Mo at 0 and 300 GPa (left and right panels, respectively). The *s* valence band (energy between −8 and −7 eV at the Γ point) rises in energy more quickly than *d* valence bands with increasing pressure.

sons with experimental data that can be made. It is particularly important in the context of melting calculations, because, for the harmonic solid, errors in phonon frequencies translate directly into free-energy errors, which are linked with errors in melting temperature. We present here our calculations of the phonon dispersion relations of Mo at its experimental volume, using PAW with GGA(PBE) exchange-correlation.

The technique for calculating the phonon frequencies is the small displacement method,[41] as implemented in our PHON code,[50] which we used in earlier work on Fe, Al, and Cu. In this method, the elements of the force-constant matrix are obtained by displacing atoms from the perfect-lattice positions and computing by DFT the forces on all the atoms. For a bcc crystal, it suffices to displace a single atom along the (111) direction. Since all the calculations employ periodic boundary conditions, the displaced atom is at the center of a periodically repeated supercell. To obtain accurate dispersion relations over the whole Brillouin zone, this supercell must be large enough so that the elements of the force-constant matrix have negligible values at its boundaries. In addition, the calculation of the forces must be converged with respect to electronic **k**-point sampling, and to enhance this convergence we employ Fermi smearing. This smearing itself incurs errors, which need to be made negligible. In summary, the phonon frequencies must be converged with respect to atom displacement, supercell size, **k**-point sampling, and Fermi smearing. Rather than insisting that every single frequency be converged, it is more convenient to require that the geometric mean frequency $\overline{\omega}$ be converged. This quantity is defined by the equation

$$\ln \overline{\omega} = \frac{1}{N_{\mathbf{q}i}} \sum_{\mathbf{q},i} \ln(\omega_{\mathbf{q}i}), \qquad (6)$$

where $\omega_{\mathbf{q}i}$ is the phonon frequency of branch i at wave vector $\mathbf{q}$, and $N_{\mathbf{q}i}$ is the number of branches times total number of $\mathbf{q}$ points in the sum. It is useful to work with $\overline{\omega}$, because it is directly related to the harmonic free energy of lattice vibrations, which, well above the Debye temperature, is equal to $3k_BT \ln(\hbar\overline{\omega}/k_BT)$ per atom.

Our aim is to have $\overline{\omega}$ converged to better than 1% with respect to all technical parameters. Tests on small supercells show that an atomic displacement of 0.0062 Å is small enough to ensure that anharmonic errors are well below this tolerance. To test convergence with respect to **k**-point sampling and Fermi smearing width σ, we have done extensive tests on a $2\times2\times2$ supercell containing 8 atoms (see Table I). These tests show that for $\sigma=0.7$ eV, it is easy to achieve excellent **k**-point convergence. But, repetition of this at $\sigma=0.5$ eV reveals that this reduction of σ causes $\overline{\omega}$ to change by ~1 %. However, further reduction of σ to 0.3 eV changes $\overline{\omega}$ by less than 0.5%, so that $\overline{\omega}$ appears to be adequately converged with respect to **k** points and σ with a $12\times12\times12$ **k**-point grid and $\sigma=0.5$ eV. We then seek convergence with respect to supercell size using this value of σ and a **k**-point density that is reduced in inverse proportion to su-

TABLE I. Convergence of mean phonon frequency $\overline{\omega}$ [see Eq. (6)] with supercell size, **k** grid, and Fermi broadening σ.

N	Supercell	**k** grid	σ (eV)	$\overline{\omega}$ (10^{12} s^{-1})
8	$2\times2\times2$	$4\times4\times4$	0.7	20.734
		$8\times8\times8$	0.7	21.385
		$12\times12\times12$	0.7	21.204
		$16\times16\times16$	0.7	21.206
8	$2\times2\times2$	$8\times8\times8$	0.5	21.498
		$12\times12\times12$	0.5	21.045
		$16\times16\times16$	0.5	21.037
		$24\times24\times24$	0.5	21.045
8	$2\times2\times2$	$8\times8\times8$	0.3	21.703
		$12\times12\times12$	0.3	20.921
		$16\times16\times16$	0.3	20.811
		$24\times24\times24$	0.3	20.951
		$32\times32\times32$	0.3	20.941
64	$4\times4\times4$	$6\times6\times6$	0.5	21.699
216	$6\times6\times6$	$4\times4\times4$	0.5	21.727

percell size. The results indicate that convergence to our required tolerance is achieved with the $4\times4\times4$ supercell of 64 atoms.

Figure 5 shows a comparison with experimental data of our calculated phonon frequencies obtained with the $6\times6\times6$ supercell of 216 atoms, a $4\times4\times4$ **k**-point grid, and $\sigma=0.5$ eV. According to our convergence tests, any discrepancy with experimental frequencies of over 1% represents a genuine disagreement. The agreement is actually very satisfactory over most of the Brillouin zone, with typical discrepancies being 1%–2%. However, there is a region around the H point $\mathbf{k}=(2\pi/a_0)(1,0,0)$, where there are discrepancies of ~5%. This same H-point problem has been noted by previous authors who dealt with transition metals (Mo and Nb) and used pseudopotential-based methods.[52–54] The origin of this sharp dip in the phonon dispersion curve of Mo at point H has been related to the nesting of electronic states near the Fermi level[55–57] (see the figures in Sec. III B), so it is likely that by reducing the Fermi smearing and increasing the number of **k** points the agreement with experiments would be improved. In any case, we believe that since the discrepan-
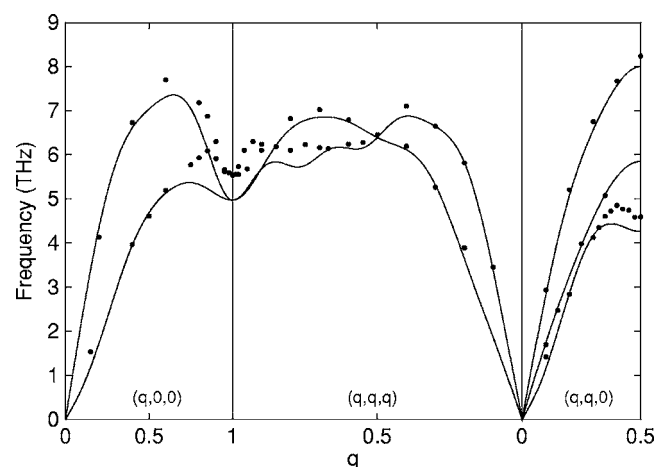

FIG. 5. Comparison of calculated (curves) and experimental (solid squares) phonon dispersion relations of Mo at zero pressure. Experimental data are from Ref. 51.

cies are rather localized in **k** space, they will have only a weak effect on the thermodynamic properties of the system.

D. Conclusions from the tests

In summary, our tests show that: (i) neither LDA nor GGA perfectly reproduces the experimental $T=0$ K pressure-volume curve, but the volume given by GGA deviates by only a small and almost constant amount of $\sim 1.5\%$ from the experimental value over the pressure range 0–300 GPa; (ii) with GGA, the inclusion of $4s$ states in the valence set makes a negligible difference to the $P(V)$ curve; (iii) comparisons of PAW and FP-LAPW confirm the accuracy of PAW for both $P(V)$ and the electronic DOS, and in particular PAW accurately reproduces the well-known pressure induced shift of s-p bands relative to d bands; (iv) GGA gives rather accurate phonon frequencies over most of the Brillouin zone. This evidence provides a firm basis for our calculations on the high-pressure melting of Mo, which employ the PAW technique with GGA(PBE) exchange-correlation, and with $4p$ states but not $4s$ states in the valence set.

IV. MELTING

We begin this section by presenting our *ab initio* calculations of the melting curve of Mo using the reference coexistence technique (see Sec. II B); our results for the volume and entropy changes on melting as a function of pressure are also reported. In Sec. IV B, we outline our calculations of the atomic and electronic structures of the bcc solid and the liquid.

A. Calculation of melting curve

We start by determining the *ab initio* T_m at a pressure close to zero. At this pressure, we have experimental values for T_m (2883 K) (Ref. 58) and the volumes per atom of coexisting solid and liquid (16.34 and 17.04 Å/atom).[58] We use this information to set the temperature and volume/atom of the *ab initio* MD simulations that we performed to fit the parameters of the reference model. These MD simulations employed systems of 125 atoms with Γ-point sampling, and were done at $T=2800$ K, $V=16.34$ Å^3/atom (solid), and $T=3000$ K, $V=16.34$ Å^3/atom (liquid). The starting configuration of the solid was produced by equilibrating the system, which initially was in the perfect crystal configuration, to temperature 2800 K. For the liquid, we produced the starting configuration by raising the temperature of the perfect crystal to 8000 K (more than twice the experimental T_m) and then rethermalizing it again to 3000 K. We checked that the system was in the liquid state by monitoring the time-dependent mean-squared displacement. The durations of the simulations were about 2 ps for the solid and 4 ps for the liquid. A set of 100 solid and liquid configurations from these *ab initio* simulations was then used to fit the reference model by varying the EAM parameters to minimize the dimensionless quantity ψ and the pressure difference ΔP (see Sec. II B). The resulting EAM parameters are reported in Table II. The very small value $\psi = 0.078$ indicates a good quality of fit, and the ΔP values of 0.3 and 0.7 GPa for the liquid and solid, respectively, were also satisfactory (these ΔP give contributions of

TABLE II. Parameters of the EAM potential deduced for Mo and used for the coexistence simulations. Values are obtained by fitting to *ab initio* simulations on solid and liquid.

P (GPa)	ε (eV)	a (Å)	n	m	C
0–100	0.323	3.579	5.93	3.72	12.66
100–200	0.169	4.985	4.96	3.88	28.08
200–400	0.144	4.760	5.07	3.78	26.90

only 7 and 3×10^{-5} eV/atom to ΔG). We then performed reference coexistence simulations, and found that the solid and liquid remain in stable coexistence over periods of 60 ps at $P=11$ GPa and $T=3260$ K. To illustrate this, we show in Fig. 6 the density profile obtained by calculating the number of atoms in slices parallel to the solid-liquid interface. The solid is immediately recognizable from the regular oscillations with a repeat distance of 2.75 Å (equal to $\sqrt{3}/2$ times the lattice parameter of the bcc lattice, corresponding to the distance between nearest neighbors), whereas the density profile is flat in the liquid region. Finally, we corrected for the difference between *ab initio* and reference energy functions, obtaining a final *ab initio* $T_m=3205$ K at $P=11$ GPa. The values of $\langle \Delta U \rangle_{\text{ref}}^{ls}/N$ (where $\langle \Delta U \rangle_{\text{ref}}^{ls} \equiv \langle \Delta U \rangle_{\text{ref}}^{l} - \langle \Delta U \rangle_{\text{ref}}^{s}$) and of $\langle (\delta \Delta U)^2 \rangle_{\text{ref}}/2Nk_{\text{B}}T$ of the liquid and solid used to make these corrections are reported in Table III. We comment below on the volume and entropy of melting.

We now use the reference model to obtain a first estimate of the melting curve at higher pressures. Reference coexistence simulations performed with the EAM parameters from the fit at $P \simeq 0$ GPa showed that at $P=92$ GPa, the reference T_m is 5392 K, the volumes of coexisting solid and liquid being 13.30 and 13.53 Å^3/atom. Correcting for the differences between *ab initio* and reference energy functions, we obtain the *ab initio* melting temperature $T_m=4867$ K at $P=92$ GPa. We note that the correction to T_m is considerably greater than at $P \simeq 10$ GPa, but we believe it is still small enough for the first-order correction scheme to remain valid, and this is confirmed by subsequent results (see below).
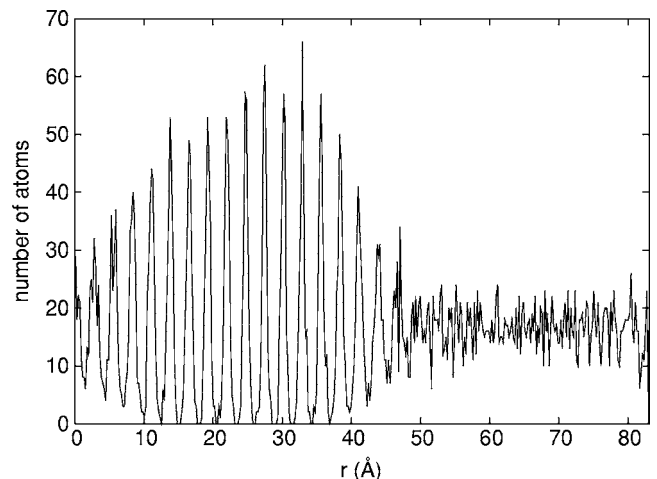

FIG. 6. Density profile in simulation of coexisting solid and liquid Mo at $P=11$ GPa, $T=3260$ K after 60 ps. The simulation is performed with the embedded-atom reference model on a system of 6750 atoms.

TABLE III. Difference $\langle\Delta U\rangle_{\text{ref}}^{ls}\equiv\langle\Delta U\rangle_{\text{ref}}^{l}-\langle\Delta U\rangle_{\text{ref}}^{s}$ between the liquid and solid thermal averages of the difference $\Delta U\equiv U_{\text{AI}}-U_{\text{ref}}$ of *ab initio* and reference energies, and thermal averages in solid and liquid $\langle(\delta\Delta U)^2\rangle_{\text{ref}}$ of the squared fluctuations of $\delta\Delta U\equiv\Delta U-\langle\Delta U\rangle_{\text{ref}}$, with averages evaluated in the reference system and normalized by dividing by the number of atoms N. Melting temperatures for the reference and *ab initio* systems are also reported.

$T_{\text{m}}^{\text{ref}}$ (K)	$\langle\Delta U\rangle_{\text{ref}}^{ls}/N$ (eV/atom)	$\frac{1}{2}\beta\langle(\delta\Delta U)^2\rangle_{\text{ref}}/N$ (eV/atom)		T_{m}^{AI} (K)
		Solid	Liquid	
3260	0.009(2)	0.038(2)	0.032(2)	3205
5392	0.027(1)	0.024(2)	0.028(1)	4867
6510	0.038(1)	0.035(3)	0.030(2)	5969
7324	0.002(1)	0.023(2)	0.015(2)	7281
8618	0.013(1)	0.018(2)	0.032(2)	8154

However, when we repeated this procedure at $P\simeq 160$ GPa, still using the reference model fitted at $P\simeq 0$, we found that the corrections need to go from reference to *ab initio* T_m were even larger, and we considered it essential to refit the reference model. Rather than attempting to do this refit at $P\simeq 160$ GPa, we returned to $P\simeq 90$ GPa, where our knowledge of the *ab initio* T_m is reasonably secure. The refitting at $P\simeq 90$ GPa produced the new parameters reported in Table II ($100\leq P\leq 200$ GPa). This new reference model, when used in coexistence simulations at $P=156$ GPa, yielded the reference $T_m=6510$ K, and a corrected *ab initio* value $T_m=5969$ K. We regarded the size of this correction as acceptably small. In a similar way, when we performed calculations at $P\simeq 270$ GPa, using the reference model fitted at 90 GPa, the corrections were unacceptably large, and we performed a refit at 160 GPa. This refitted reference model required only rather small corrections when used at 270 and 380 GPa.

The reference and *ab initio* T_m as a function of pressure from this full set of calculations are reported in Fig. 7. We find that the *ab initio* T_m values can be very well fitted with the so-called Simon equation[60] $T_m=a(1+P/b)^c$, with $a=2894$ K, $b=37.22$ GPa, and $c=0.433$. The resulting $P=0$ melting temperature of 2894 K is very close to the experimental value of 2883 K. Using the Simon equation, we can obtain the melting slope dT_m/dP at any pressure. At $P=0$, we find $dT_m/dP=33.7$ K GPa^{-1}, which agrees closely with the experimental value[58] of 33.3 K GPa^{-1}. Also shown in Fig. 7 is the point on the melting curve at $P\simeq 375$ GPa estimated from the shock data of Hixson *et al.*,[4] which is close to our melting curve. The diamond anvil cell (DAC) measurements of Errandonea *et al.*[1] differ greatly from our results, since their dT_m/dP is essentially zero over most the range from 0 to 100 GPa. Previous theoretical melting curves[6,9] for Mo, also shown in the figure, are in general agreement with our results, though there are substantial quantitative differences. The comparison of all these experimental and theoretical results raises important issues, which will be discussed in Sec. V.

The entropy and volume of fusion of the reference model, denoted by S_{ref}^{ls} and V_{ref}^{ls}, are straightforward to calculate. From the reference coexistence simulations, we have (P,T) pairs lying on the reference melting curve. We then perform separate single-phase MD simulations of the solid
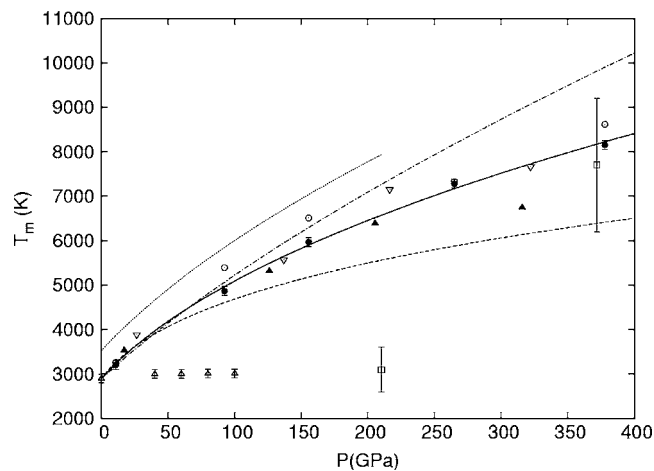

FIG. 7. Calculated *ab initio* melting curve (filled circles and solid line) of this work compared with previous results: generalized pseudopotential calculations of Moriarty (Ref. 6, dotted line), dislocation-mediated models of Belonoshko *et al.* (Ref. 9, long-dashed line), and Verma *et al.* (Ref. 59, dashed-dotted line); experimental shock-wave (Ref. 4) and DAC (Ref. 1) measurements are shown with empty squares and triangles, respectively. Filled and inverted-empty triangles show solid and liquid *ab initio* molecular dynamics calculations of Belonoshko *et al.* (Ref. 9), respectively. Empty circles show results of this work obtained with the EAM model without free-energy corrections.

and liquid reference systems at chosen temperatures, using systems of 3375 atoms, adjusting the volumes in each case to give the appropriate P. The difference of the resulting volumes give us V_{ref}^{ls}. At the same time, the simulations give the internal energy U, from which we obtain the enthalpies $H=U+PV$ of the two phases. Then, the difference of enthalpies H_{ref}^{ls} gives us the entropy difference, since $TS_{\text{ref}}^{ls}=H_{\text{ref}}^{ls}$. We find that S_{ref}^{ls} is almost constant along the reference melting curve, going from 0.58 k_B/atom at $P\sim 0$ to 0.69 k_B/atom at $P=378$ GPa. Since the reference system mimics the *ab initio* system rather closely, we assume that S_{AI}^{ls} for the *ab initio* system is essentially the same as S_{ref}^{ls}. To obtain the *ab initio* volume of fusion V_{AI}^{ls}, we use the Clausius-Clapeyron relation $dT_m/dP=V_{\text{AI}}^{ls}/S_{\text{AI}}^{ls}$. Our V^{ls} results for the reference and *ab initio* systems as a function of P are reported in Fig. 8. We
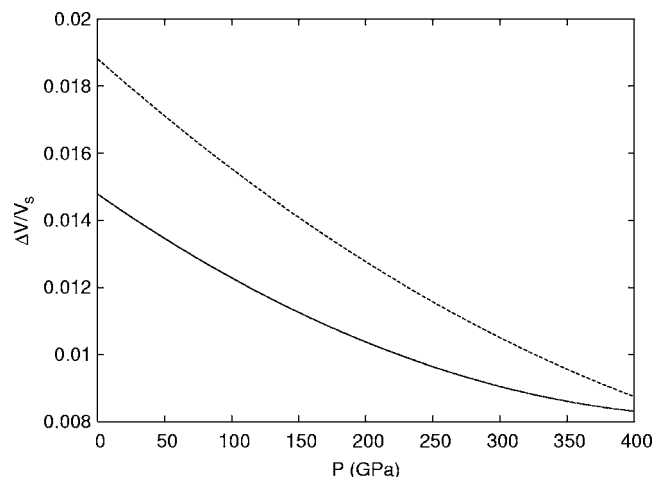

FIG. 8. *Ab initio* fractional volume change on melting of Mo as a function of pressure. Solid and dashed curves: present work, with and without free-energy correction, respectively.
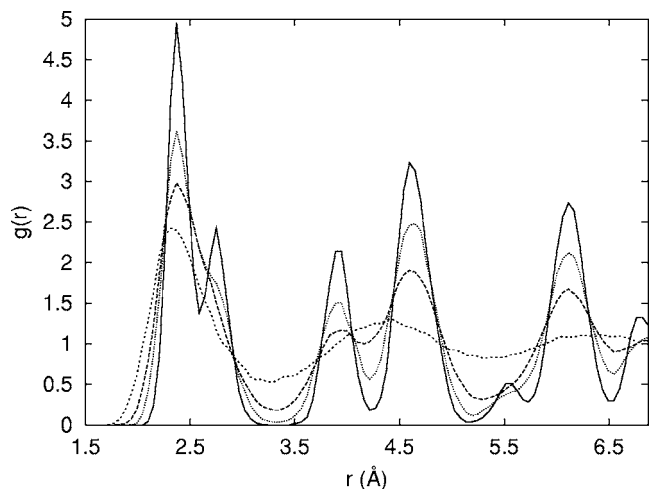
FIG. 9. Calculated radial distribution function of Mo for: solid at P = 212 GPa and T = 2000 K (solid line), solid at P = 216 GPa and T = 4000 K (dotted line), solid at P = 230 GPa and T = 6000 K (long-dashed line) and liquid at P = 224 GPa and T = 7500 K (short-dashed line).

note that in both cases the fractional volume change V^{ls}/V^s decreases smoothly from ∼1.5 % at P = 0 to ∼0.9 % at 400 GPa.

B. Atomic and electronic structure of solid and liquid

We noted in the Introduction that theories of the melting of bcc transition metals sometimes assume[20] that melting is associated with a significant change of coordination number, so that the electronic density of states should also change markedly. In order to test these ideas for Mo, we have calculated the radial distribution function $g(r)$ of Mo from a series of AIMD simulations of the solid and the liquid performed at $P \simeq 216$ GPa. The simulations were all done with 125 atoms, and had a typical duration of 2 ps after equilibration. Figure 9 reports our calculated $g(r)$ at T = 2000, 4000, and 6000 K (solid state), and at T = 7500 K (liquid state); we recall (Fig. 7) that our calculated T_m at this pressure is 6641 K. At 2000 K, the shells containing 8 first neighbors and 6 second neighbors at distances of r = 2.44 and 2.81 Å

are clearly separated, and $g(r)$ goes to zero at $r \simeq 3.4$ Å, between the second and third shells. However, at T = 4000 K, the first and second shells have already merged, though the shoulder due to the second shell is clearly visible. The $g(r)$ of the solid at T = 6000 K presents similar trends to those shown at 4000 K, the main difference being that the valley between the second and third atomic shells now clearly moves upwards from zero. The change in $g(r)$ in going from the solid at T = 6000 K to the liquid at 7500K is substantial for r > 3 Å, with the well-defined peaks due to third and higher neighbors in the solid becoming heavily broadened. However, the peak closest to the origin does not suffer a large change. We define the coordination number N_c in the usual way as $N_c = 4\pi\bar{\rho}\int_0^{r_c}g(r)r^2 dr$, with $\bar{\rho}$ the bulk number density and r_c the distance of the first minimum. The r_c values at the four temperatures are 3.41, 3.41, 3.41, and 3.31 Å, and the resulting N_c values are 14, 14, 14, and 13.35. Apart from the expected increase in disorder, the main change on going from solid to liquid is thus a slight *decrease* in coordination number. We comment further on this in Sec. V.

Turning now to the electronic density of states (DOS), we present first our AIMD results for P in the range 50–70 GPa at a series of temperatures, the simulations being performed on a system of 125 atoms with Γ-point sampling. The typical duration of these simulations was 2 ps after equilibration and the DOS were calculated by averaging over 150 different configurations. We report in Fig. 10 the calculated DOS at the thermodynamic states given by (P,T) = (48,0), (50,2000), (51,3300) for the solid, and (P,T) = (72,5000) for the liquid (units of GPa and K). (Our *ab initio* T_m for 50 < P < 70 GPa are in the range 4185–4577 K.) We have checked in each case that the system is in the solid or liquid states by looking at the mean-squared displacement and structure factor. We note the progressive broadening of the DOS peaks with increasing thermal disorder in the solid, an effect which continues further in the liquid. The Fermi-level value of the DOS increases slightly on melting. As far as occupied states are concerned, melting appears to cause a slight redistribution of d states from lower in the band to the region of the Fermi level.
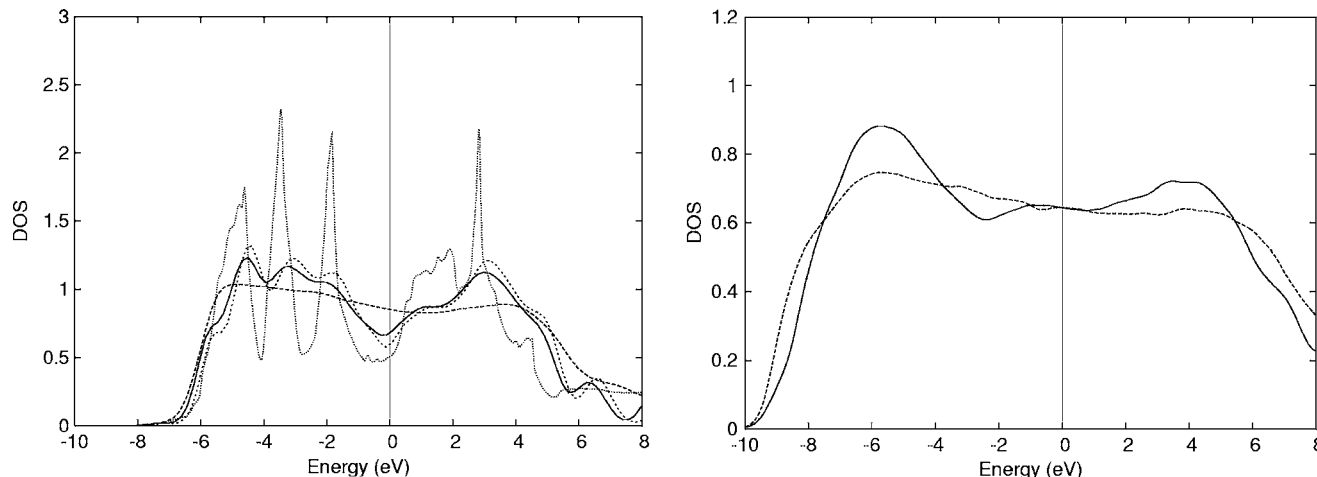

FIG. 10. Density of valence electronic states of Mo at finite temperature and on melting. Left: solid at P = 48 GPa and T = 0 K (dotted line), solid at P = 50 GPa and T = 2000 K (short-dashed line), solid at P = 51 GPa and T = 3300 K (solid line) and liquid at P = 72 GPa and T = 5000 K (long-dashed line). Right: solid at P = 285 GPa and T = 7000 K (solid line) and liquid at P = 300 GPa and T = 8250 K (dashed line). Fermi energy levels are shifted to zero.

In the right-hand panel of Fig. 10, we compare our AIMD results for the electronic DOS at the solid state-point $(P,T)=(285,7000)$ and the liquid state-point $(P,T)=(300,8250)$ (units of GPa and K), which are just below and just above our calculated melting curve. We note the rather minor changes caused by melting. Interestingly, the Fermi-level value of the DOS is almost identical in the two phases at this pressure. The relationship of these results with earlier work on the electronic structure of liquid transition metals will be discussed in the following section.

V. DISCUSSION AND CONCLUSIONS

At the start of this paper, we emphasized the large discrepancies between melting curves of transition metals derived from static compression and shock measurements, and we mentioned that previous DFT work on Mo supports the shock measurements. The present work fully confirms that the melting curve predicted by DFT in the PBE approximation for exchange-correlation energy lies far above the static compression measurements, but at high pressures is consistent with the shock data. This confirmation is important, because of deficiencies or uncertainties in previous DFT work. The reliability of the present calculations is supported by our close agreement with the experimental $P=0$ values of both the melting temperature T_m and the melting slope dT_m/dP. Our melting curve is below the theoretical curve of Moriarty[6] by ~600 K at $P=0$, and this difference increases with increasing P. However, this is not surprising, since the generalized pseudopotential model that he used is known to disagree with experimental phonon frequencies, and because he included thermal electronic excitations only approximately. In the present work, we have taken pains to verify the accuracy of the phonon frequencies given by our methods, and thermal electronic excitations are fully included within our DFT framework. Perhaps more surprising is that our melting curve agrees closely with that obtained by Belonoshko et al.[9] using direct DFT MD simulation. This is unexpected, since they believed that their melting curve suffered from a substantial superheating error of ~20%. The close agreement suggests that they may have been unduly pessimistic, and this point deserves further investigation. We included in Fig. 7 the results of Belonoshko et al.[9] and of Verma et al.[59] obtained by the dislocation-mediated theory of melting.[61,62] It is not clear to us whether one can expect a theory of melting based exclusively on the properties of the solid to be fully reliable. One of the problems with this approach is that the predicted melting curves rely on thermodynamic data that may not be reliably known. The rather large differences between the two melting curves based on the dislocation theory may be indicative of the limited reliability of this approach.

The change of volume on melting of ~1% given by our calculations is small, but still much greater than the volume change implied by the static compression values[1,10,20] of dT_m/dP. Arguments in favor of a very low volume change based on a significant increase of coordination number on going from bcc solid to melt appear to be incorrect, according to our DFT MD calculations of the radial distribution function $g(r)$. We find only rather minor differences between $g(r)$ for high-T solid and melt. In particular, there is actually a slight *decrease* in coordination number from 14 to ~13 on melting, so that the liquid is slightly less close packed than the solid. We comment that ideas based on hard-sphere packing are likely to be misleading, since the repulsive interactions between Mo atoms at high T are rather soft (see below).

We mentioned in the Introduction the recent theory of Ross et al.,[20] according to which a very low melting slope is expected for bcc transition metals. The theory invokes the well-known transfer of electrons from s-p to d states with increasing compression, and the fact that this transfer depends on crystal structure. In applying this theory to the melting of Mo, the authors estimated the effective number of d electrons n_d by treating the high-temperature solid as a perfect bcc crystal and the liquid as a perfect fcc crystal. They also assumed that a change of n_d on melting will be associated with a change of d bandwidth. They found that the changes of electronic structure stabilize the liquid relative to the solid, and yield a major reduction of T_m. In considering this theory in the light of the results we have presented, it is important to appreciate that our calculations are all based on an accurate implementation of DFT. As in all simulations using Born-Oppenheimer DFT MD, the VASP code recalculates the entire self-consistent electronic structure at every time step of the time evolution. As described in Sec. III B, we have gone to considerable lengths to show that the PAW implementation of DFT used in our MD yields results for the electronic DOS which are almost indistinguishable from those given by the FP-LAPW technique, which is one of the most accurate available. This means that all the effects that enter the theory of Ross et al.,[20] including s-p to d electron transfer and changes of d bandwidth, are fully included in our simulations. Nevertheless, we do not obtain the very low melting slope that they predict. The reason for this is presumably that their treatment of the high-T solid and the liquid as perfect crystals is incorrect. As we have seen, their assumption of a large structural change on melting also appears to be questionable. This point is reinforced by our finding that the electronic DOS changes only slightly on melting, especially at high P.

We end this discussion by commenting on the embedded-atom model (EAM) used as a reference system in determining the melting curve. It is an important finding of this work that the EAM is able to mimic accurately the DFT total-energy function of solid and liquid close to coexistence. This does not mean, however, that we accept the melting curve of the reference model as the true melting curve. This could be dangerous, because we might then miss d-band electronic effects that were not explicitly included in the model. However, in our procedure, any such effects are automatically picked up in the corrections that we apply, since these explicitly account for free-energy differences between the reference and DFT systems. We note in passing that the fitting of our reference model yields parameters that resemble those we found in our earlier work on the melting of Fe.[15] In particular, the inverse-power repulsive potential in our present EAM model has an exponent n close to 6 at low P, decreasing to ~5 at high P. For comparison, the fitted

EAM in our Fe work had $n = 5.9$, which is very similar. We are currently investigating the systematic behavior of EAM parameters in solid and liquid transition metals at high P and T, and we hope to report on this elsewhere.

The main conclusions from this work are as follows. Our DFT calculations of the melting curve of Mo up to 400 GPa fully confirm earlier work showing that the DFT melting curve is consistent with shock data, but is far above the melting curve given by static compression experiments. Our calculations indicate that at high P there are only minor changes of both atomic and electronic structure on going from the high-temperature bcc solid to the melt. Suggested mechanisms for an anomalously low melting slope dT_m/dP of Mo based on transfer of electrons from s-p states to d states appear to be incompatible with the present DFT calculations. This tends to confirm earlier suggestions[9] that the transition identified as melting in high-P static compression experiments may not be true thermodynamic melting.

ACKNOWLEDGMENTS

[1] D. Errandonea, B. Schwager, R. Ditz, C. Gessmann, R. Boehler, and M. Ross, Phys. Rev. B **63**, 132104 (2001).

[2] D. Errandonea, M. Somayazulu, D. Häusermann, and D. Mao, J. Phys. Condens. Matter **15**, 7635 (2003).

[3] J. M. Brown and J. W. Shaner, in *Shock Waves in Condensed Matter 1983*, edited by J. R. Assay, R. A. Graham, and G. K. Straub (Elsevier, Amsterdam, 1983), p. 91.

[4] R. S. Hixson, D. A. Boness, J. W. Shaner, and J. A. Moriarty, Phys. Rev. Lett. **62**, 637 (1989).

[5] R. S. Hixson and F. N. Fritz, J. Appl. Phys. **71**, 1721 (1992).

[6] J. A. Moriarty, Phys. Rev. B **49**, 12431 (1994).

[7] J. A. Moriarty, J. F. Belak, R. E. Rudd, P. Söderlind, F. H. Streitz, and L. H. Yang, J. Phys.: Condens. Matter **14**, 2825 (2002).

[8] Y. Wang, R. Ahuja, and B. Johansson, Phys. Rev. B **65**, 014104 (2001).

[9] A. B. Belonoshko, S. I. Simak, A. E. Kochetov, B. Johansson, L. Burakovsky, and D. L. Preston, Phys. Rev. Lett. **92**, 195701 (2004).

[10] D. Errandonea, Physica B (Amsterdam) **357**, 356 (2005).

[11] M. J. Gillan, D. Alfè, J. Brodholt, L. Vočadlo, and G. D. Price, Rep. Prog. Phys. **69**, 2365 (2006).

[12] D. Alfè, M. J. Gillan, and G. D. Price, Nature **401**, 462 (1999).

[13] A. B. Belonoshko, R. Ahuja, and B. Johansson, Phys. Rev. Lett. **84**, 3638 (2000).

[14] A. Laio, S. Bernard, G. L. Chiarotti, S. Scandolo, and E. Tosatti, Science **287**, 1027 (2000).

[15] D. Alfè, G. D. Price, and M. J. Gillan, Phys. Rev. B **65**, 165118 (2002).

[16] L. Vočadlo and D. Alfè, Phys. Rev. B **65**, 214105 (2002).

[17] D. Alfè, Phys. Rev. B **68**, 064423 (2003).

[18] L. Vočadlo, D. Alfè, G. D. Price, and M. J. Gillan, J. Chem. Phys. **120**, 2872 (2004).

[19] L. J. Wittenberg and R. DeWitt, J. Chem. Phys. **56**, 4526 (1972).

[20] M. Ross, L. H. Yang, and R. Boehler, Phys. Rev. B **70**, 184112 (2004).

[21] D. G. Pettifor, J. Phys. F **7**, 613 (1977).

[22] D. G. Pettifor, Solid State Phys. **40**, 43 (1987).

[23] J. A. Moriarty, Phys. Rev. B **42**, 1609 (1990).

[24] D. Alfè, M. J. Gillan, and G. D. Price, J. Chem. Phys. **116**, 6170 (2002).

[25] M. S. Daw and M. I. Baskes, Phys. Rev. B **29**, 6443 (1984).

[26] M. W. Finnis and J. E. Sinclair, Philos. Mag. A **50**, 45 (1984).

[27] R. M. Martin, *Electronic Structure* (Cambridge University Press, Cambridge, 2004).

[28] J. Kohanoff, *Electronic Structure Calculations for Solids and Molecules: Theory and Computational Methods* (Cambridge University Press, Cambridge, 2006).

[29] T. Gu, J. Qin, C. Xu, and X. Bian, Phys. Rev. B **70**, 144204 (2004).

[30] P. E. Blöchl, Phys. Rev. B **50**, 17953 (1994).

[31] G. Kresse and D. Joubert, Phys. Rev. B **59**, 1758 (1999).

[32] D. Vanderbilt, Phys. Rev. B **41**, 7892 (1990).

[33] O. K. Andersen, Phys. Rev. B **12**, 3060 (1975).

[34] D. D. Koelling and G. O. Arbman, J. Phys. F **5**, 2041 (1975).

[35] D. Singh, *Planewaves, pseudopotentials and the LAPW-method* (Kluwer Academic, Dordrecht, 1994).

[36] D. D. Koelling and B. N. Harmon, J. Phys. C **10**, 3107 (1977).

[37] G. Kresse and J. Furthmüller, Phys. Rev. B **54**, 11169 (1996).

[38] P. Blaha, K. Schwarz, G. K. Madsen, D. Kvasnicka, and J. Luitz, *WIEN2k: An Augmented Plane Wave plus Local Orbital Program for Calculating Crystal Properties* (Technical University of Vienna, Vienna, 2001).

[39] N. D. Mermin, Phys. Rev. **137**, A1441 (1965).

[40] D. Alfè, G. D. Price, and M. J. Gillan, Phys. Rev. B **64**, 045123 (2001).

[41] G. Kresse, J. Furthmüller, and J. Hafner, Europhys. Lett. **32**, 729 (1995).

[42] S. Nosé, Mol. Phys. **52**, 255 (1984).

[43] D. M. Ceperley and B. I. Alder, Phys. Rev. Lett. **45**, 566 (1980).

[44] J. P. Perdew, K. Burke, and M. Ernzerhof, Phys. Rev. Lett. **77**, 3865 (1996).

[45] In order to ensure energy convergence to within 1 meV/atom in the WIEN2K calculations, we use the following settings: tolerance for energy convergence in the self-consistency cycle: 1×10^{-4} eV; muffin-tin radius (R_{MT}) ranges from 1.32 Å for the largest atomic volume to 1.15 Å for the smallest; plane-wave cutoff $K_{max} = 9.5/R_{MT}$; maximum angular momentum component for partial waves used inside atomic spheres $L_{max} = 10$; number of wave vectors in full Brillouin zone for **k**-point sampling $= 3000$; $4p$ and $4s$ states are treated as valence states throughout.

[46] Z. Wu and R. E. Cohen, Phys. Rev. B **73**, 235116 (2006).

[47] P. S. Svendsen and U. von Barth, Phys. Rev. B **54**, 17402 (1996).

[48] J. H. Wood, Phys. Rev. **126**, 517 (1962).

[49] A. R. Miedema, P. F. Chatel, and F. R. de Boer, Physica B (Amsterdam) **100**, 1 (1980).

[50] D. Alfè, 1998, Program available at http://chianti.geol.ucl.ac.uk/~dario

[51] J. Zarestky, C. Stassis, B. N. Harmon, K. M. Ho, and C. L. Fu, Phys. Rev. B **28**, 697 (1983).

[52] P. Oelhafen, R. Wahrenberg, and H. Stupp, J. Phys.: Condens. Matter **12**, 9 (2000).

[53] K. M. Ho, C. L. Fu, B. N. Harmon, W. Weber, and D. R. Hamman, Phys. Rev. Lett. **49**, 673 (1982).

[54] K. M. Ho, C. L. Fu, and B. N. Harmon, Phys. Rev. B **29**, 1575 (1984).

[55] C. M. Varma and W. Weber, Phys. Rev. Lett. **39**, 1094 (1977).

[56] C. M. Varma and W. Weber, Phys. Rev. B **19**, 6142 (1979).

[57] S. K. Mahna, Czech. J. Phys. **37**, 881 (1987).

[58] J. W. Shaner, G. R. Gathers, and C. Minichino, High Temp. - High Press. **9**, 331 (1977).

[59] A. K. Verma, R. S. Rao, and B. K. Godwal, J. Phys.: Condens. Matter **16**, 4799 (2004).

[60] F. E. Simon and G. Glatzel, Z. Anorg Allg. Chem. **178**, 309 (1929).

[61] L. Burakovsky, D. L. Preston, and R. R. Silbar, J. Appl. Phys. **88**, 6294 (2000).

[62] D. L. Preston and D. C. Wallace, Solid State Commun. **81**, 277 (1992).